Radiocarbon, Vol 00, Nr 00, 2020, p 1–15 DOI:10.1017/RDC.2019.154

^{14}C DATED CHRONOLOGY OF THE THICKEST AND BEST RESOLVED LOESS/PALEOSOL RECORD OF THE LGM FROM SE HUNGARY BASED ON COMPARING PRECISION AND ACCURACY OF AGE-DEPTH MODELS

Pál Sümegi[1,2,3]* • Sándor Gulyás[1,3] • Dávid Molnár[1,3] • Gábor Szilágyi[1,4] • Balázs P Sümegi[1,5] • Tünde Törőcsik[1,3,5] • Mihály Molnár[5]

[1]Department of Geology and Palaeontology, University of Szeged, 6722 Szeged, Egyetem Street 2, Hungary
[2]Archaeological Institute of Hungarian Academy of Sciences, Budapest, Úri street 49, Hungary
[3]University of Szeged, Interdisciplinary Excellence Centre, Institute of Geography and Earth Sciences, Long Environmental Changes Research Team, H-6722 Szeged, Egyetem u. 2-6, Hungary
[4]Hortobágy National Park, 4024 Debrecen, Sumen u. 2, Hungary
[5]Institute of Nuclear Research of HAS, 4026 Debrecen, Bem tér 18/c, Hungary

ABSTRACT. The Madaras profile found at the northernmost fringe of Bácska loess plateau is one of the thickest and best-developed last glacial loess sequences of Central Europe. The 10-m profile corresponds to a period between 29 and 12 b2k. To unravel feedback to small-scale centennial climatic fluctuations at our site, recorded in the Greenland ice and North Atlantic marine cores, construction of a reliable chronology is needed. Reliability is expressed in terms of best achievable chronological precision. Accuracy however is based on choosing the model best describing the sedimentological features of our profile. Five different age-depth models had constructed and compared relying on 15 ^{14}C dates using various statistical, probabilistic approaches to choose the model with the highest achievable precision. Accuracy was also evaluated using accumulation rates against stratigraphy. Models constructed using the computer program Bacon performed best in terms of achieving the best possible stratigraphic accuracy. Seven meters of the profile represents the period of the LGM. The average sedimentation time was 16.8 yr/cm with the highest confined to the period of the LGM. Calculated average sedimentation rates were 4 times higher than previously reported. The peak accumulation periods are dated to the nadir of the LGM.

KEYWORDS: accumulation rates, accuracy, age-depth models, ^{14}C AMS dates, loess/paleosol sequence, SE Hungary.

INTRODUCTION

Understanding the outcome and manifestation of various climatic forces in the past at a regional level is a key issue in modern Quaternary research. Loess represents one of the most comprehensive semi-continuous paleoenvironmental records in the terrestrial zone (An et al. 1990; Pécsi 1990; Pye 1995; Lu and An 1998; Kemp 2001; Porter 2001, 2007). It is also one of the most extensive types of Quaternary deposits, covering approximately 10% of the land surface (Pécsi 1990; Pye 1995).

The Madaras brickyard profile found in the northernmost fringe of the Bácska loess plateau is one of the thickest and best developed last glacial loess sequences in Hungary and Central Europe and spans the coldest period of the last glacial: The Last Glacial Maximum (LGM) (Sümegi 2005; Hupuczi and Sümegi 2010; Bokhorst et al. 2011; Sümegi et al. 2012) According to previously available ^{14}C chronological data, the 10-m-thick profile of Madaras developed between ca. 29 and 12 kyr cal BP (Sümegi et al. 2012). Following Woillard and Mook (1982) and Vandenberghe (1985), this correspond to the time of the Middle and Late Pleniglacial on the European continent and MIS 2-1 (Lisiecki and Raymo 2005).

This period has been characterized by numerous millennial-scale climatic fluctuations in the Northern Atlantic (Martinson et al. 1987; Kreveld et al. 2000; Andersen et al. 2006; Rasmussen et al. 2006; Svensson et al. 2006). Understanding how these were translated to the terrestrial realm and tackling potential leads and lags in regional responses to these climatic forcing requires the construction of reliable, independent time scales fostering

*Corresponding author. Email: sumegi@geo.u-szeged.hu.

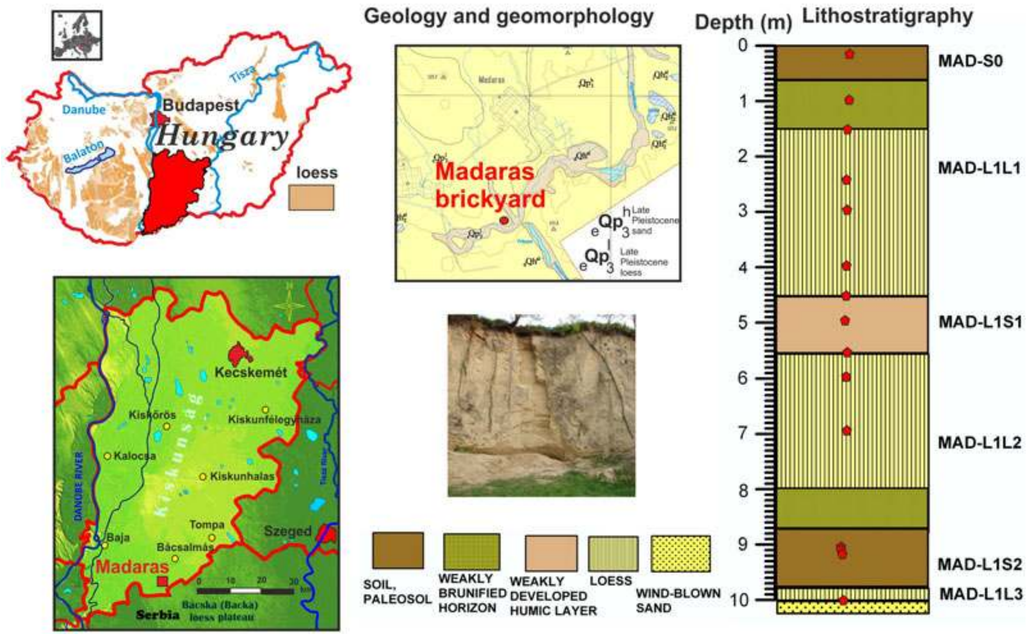

Figure 1 Location, lithostratigraphy of the studied loess/paleosol sequence of Madaras brickyard with sampling points for ^{14}C AMS dating marked.

comparison of marine and terrestrial records at high resolution. A comparison of our proxy results with other extra-regional records at the centennial scale requires the construction of reliable chronologies. As shown by Blaauw et al. (2018), age-depth model choice, dating density and quality significantly affect the precision and accuracy of our chronologies. One date per millennium provides us millennial-scale precision. Precision can be improved by increasing dating densities on the one hand (Blaauw et al. 2018). However, there are cases when lack of sufficient funding hampers the inclusion of further dates in our analysis. In these cases, a comparison of the results of age-depth models can help us assess chronological precision (Blaauw et al. 2018). According to the findings of Blaauw et al. (2018), classical age-depth models significantly underestimate uncertainty and are not improved in precision after a threshold in dating density is reached. On the other hand, Bayesian age-depth models relying on chronological ordering, as well as the fact that uncertainty is not constant between dated levels, reflecting our lack of knowledge for these depths, are more robust in providing realistic precision estimates (Blaauw et al. 2018). Although according to some, all age-depth models are wrong, but improving (Telford et al. 2004; Trachsel and Telford 2017) one should cook with what is available. Thus, assessing precision and accuracy of our models to make the best possible choice is inevitable in building chronologies. According to Blaauw et al. (2018), a minimum of 2 dates per millennium is needed for achieving millennial-scale precision using Bayesian age-depth models. But what happens if this is not feasible?

In this paper we present the first independent time scale for the referred important paleoclimatic and paleoenvironmental record of Madaras. This time scale is based on 15 ^{14}C AMS dates, which span the entire 10 m profile with relatively even distribution (Figure 1). We aim to test the chronological precision of the age-depth models built, as well as their accuracy. The former can be done through statistics (via assessing uncertainty), while the latter is an arbitrary

Table 1 Samples by type and depth as well as conventional ^{14}C ages.

Sample	Depth (cm)	Lab code	Material	BP	+/-1σ
1	16–20	D-AMS 4172	*Granaria frumentum*	10,986	57
2	100–104	D-AMS 4173	*Granaria frumentum*	13,561	41
3	148–152	DeA-1467	*Trichia hispida*	14,498	81
4	248–252	DeA-11907	*Trichia hispida*	16,133	63
5	300–304	DeA-11906	*Trichia hispida*	16,628	63
6	400–404	D-AMS 4174	*Columella columella*	17,150	50
7	448–452	DeA-11905	*Trichia hispida*	17,368	63
8	500–504	DeA-11903	*Vallonia tenuilabris*	17,858	64
9	548–552	DeA-11904	*Trichia hispida*	17,870	71
10	600–604	DeA-11901	*Euconulus fulvus*	18,942	71
11	700–704	DeA-11860	*Chondrula tridens*	20,193	93
12	896–900	DeA-11895	*Chondrula tridens*	21,381	82
13	900–908	Deb-3104*	*Pinus* charcoal	21,937	252
14	920–924	DeA-11861	*Granaria frumentum*	22,062	106
15	996–1000	D-AMS 004636	*Granaria frumentum*	34,654	264

*Conventional GPC C-14 dating at Debrecen GPC Lab.

choice based on how well the model describes the observed sedimentological features of our profile (Blaauw et al. 2018). Finally, an attempt is made to see if the chosen model is "accurate" for our needs even if inclusion of further dates to improve precision is not possible due to certain reasons.

Location and Stratigraphy of the Loess/Paleosol Sequence of Madaras

The Madaras brickyard profile is located at 46°02′14.39″N and 19°17′15.01″E, at an elevation of 131.8 m asl (Figure 1). Based on sedimentological parameters, eight sedimentary layers were distinguished within the 10 m profile exposed (Sümegi 2005; Sümegi et al. 2012) (Figure 1). The bedrock of the profile is wind-blown sand overlain by a thin layer of yellowish-brown sandy loess (MAD L1L3). On top of the loess an intensively brunified paleosol layer (9.8–8.7 m) of pale brown hue (MAD L1S2) developed, embedding charcoal fragments of Scots pine identified via anthracological examinations and dated to the transition phase of the Middle and Late Pleniglacial (Table 1). This paleosol is capped by a weakly brunified horizon between the depths of 8.7–8.0 m. These deposits are overlain by yellowish brown moderately sorted coarse sandy silts (aeolian loess) up to the depth of 5.5 m (MAD L1L2) corresponding to the terminal part of the Middle Pleniglacial. On top of this loess a weak brunified soil of light pale brown color developed embedding carbonate nodules and smaller rhizoliths (MAD L1S1). This incipient soil is overlain by light yellow sandy loess of Late Pleniglacial age up to the depth of 1.5 m (MAD L1L1). From the depth of 1.5 m a weakly brunified zone was identified grading into the topmost modern soil. The topmost 0.6 m of the studied profile corresponds to the horizon of the modern soil (MAD-SO).

MATERIAL AND METHODS

^{14}C Dating

One charcoal and 14 gastropod shell samples from the northern part of the loess wall were submitted for radiocarbon dating. AMS ^{14}C dating measurements were performed in the AMS laboratory of Seattle, WA, USA (lab code D-AMS) and Institute for Nuclear

Research of the Hungarian Academy of Sciences at Debrecen (lab code DeA-) (Table 1). The charcoal sample was measured by the Debrecen GPC Laboratory using conventional counting technique (Hertelendi et al 1989). Certain herbivorous gastropods are known to yield reliable ages for dating deposits of the past 40 ka with minimal estimates of shell age offsets on the scale of perhaps a couple of decades (Újvári et al 2014). This enables the construction of age models with resolution on the sub-centennial scale. (Sümegi and Hertelendi 1998; Pigati et al. 2004, 2010, 2013; Xu et al. 2011; Újvári et al. 2014). Based on Hungarian studies by Sümegi and Hertelendi (1998) and Újvári et al. (2014), sampled taxa were chosen accordingly (Table 1). Preparation of the samples and measurement followed the methods of Hertelendi et al. (1989 1992) and Molnár et al. (2013). Shells were ultrasonically washed and dried at room temperature. Surficial contaminations and carbonate coatings were removed by pretreatment with weak acid etching (2% HCl) before CO_2 production and graphitization. Conventional radiocarbon ages were converted to calendar ages using the software OxCal 4.2 (Bronk Ramsey 2009) and the most recent IntCal13 calibration curve (Reimer et al. 2013). Calibrated ages are reported as probability density ranges at the 2-sigma confidence level (95.4%).

Age-Depth Modeling

Taking into consideration the special pedogenetic processes and compaction during the deposition of loessy layers (Pécsi 1990), the true sedimentation rate must have varied, and thus temporal resolution must have been different from cm to cm in our study profile (Pye 1995). To count with these varying sediment accumulation rates several types of age-depth models have been applied for our dataset.

The first is the popular classical model of linear interpolation (Blaauw 2010), which assumes that accumulation rates were constant between neighboring dated depths and changed, potentially abruptly, exactly at the dated depths (Bennett 1994; Blaauw and Heegaard 2012). This model assumes a constant uncertainty between dated points, which contradicts of our lack of knowledge; i.e. higher uncertainty for these intervals. Then a classical polynomial model was also applied. All input data were from conventional ^{14}C ages. Both the linear and polynomial models were built using the software Clam yielding us ages at every cm with 95% confidence intervals (CI). Sedimentation times (year/cm) with 95% CI was also calculated.

Bayesian modeling was performed using gamma and Poisson distributions as prior information on accumulation rates. Bacon (Blaauw and Christen 2011) models the accumulation rates (AR) of many equally spaced depth sections based on an autoregressive process with gamma innovations. Inverse accumulation rates (sedimentation times expressed as year/cm) were estimated from 42 to 48 million Markov Chain Monte Carlo (MCMC) iterations, and these rates form the age-depth model. AR was first constraint by default prior information: acc. shape = 1.5 and acc. mean = 20 for the beta distribution, a memory mean = 0.7 and memory strength = 4 for beta distribution describing the autocorrelation of inverse AR. All input data were provided as ^{14}C yr BP and the model used the northern hemisphere IntCal13 calibration curve (Reimer et al. 2013) to convert conventional radiocarbon ages to calendar ages expressed as cal BP. Age modeling was run to achieve a 5-cm final resolution initially. In a second attempt to test the sensitivity of the model's boundary conditions were added based on the observed major lithostratigraphic boundaries at the level of the modern soil (1.5 m), the weak middle paleosol (4.5–5.5 m) and the lowermost pedocomplex (8–9 m).

In addition, the parameters were set as acc. shape = 2, 1.2 and acc. mean = 10, 20 for the gamma distribution and mem. mean = 0.4 and mem. strength = 10, 5, respectively. Model results with default prior information and new parameters as well as the adding of boundary conditions were compared. The fit of posterior gamma and beta distributions as well as the 95% CI ranges, plus inverse AR with 95% CI ranges were considered for comparing models. Finally, age-depth modeling was run using the set parameters. All data and figures are presented in calendar ages expressed as cal BP.

OxCal's P_sequence (Bronk Ramsey 2009) was tried with the granularity set to the size of the most dominant grain in the sequence (silt) (k = 0.3). Furthermore, to test the sensitivity, granularity (k) was also set to consider variable rates of sedimentation. In case of the latter, two sub-models were run: one without boundaries and one where stratigraphic boundaries have been introduced at 1.5, 4.5, 5.5, and 9.8 m, respectively. Ages were calculated for 1-cm intervals along with 95% CI to assess model uncertainty. Point estimates are based on the mean values.

The obtained ages of the different models (linear, polynomial, OxCal, Bacon) were evaluated for integrity and congruence as well as statistically significant differences using the non-parametric methods of pairwise Mann-Whitney U test for equality of medians and the Kolmogorov-Smirnov test for equality of distributions (Sokal and Rohlf 1995). In addition, mean 95% confidence ranges and maximum and minimum confidence values have also been calculated and compared to assess similarities and differences in uncertainty of ages (precision) for different parts of the profile. The fit of priors and posteriors in our Bayesian models was also a key to selecting the model with best chronological precision. These approaches however enabled us to test the chronological precision of the models alone (Blaauw et al. 2018). Accuracy was chosen according to the fit of the accumulation rates with our profile's stratigraphic characteristics (Blaauw et al. 2018).

Sedimentation Rates

Sedimentation rates (mm/yr) are generally calculated using the equation

$$AR = d_2\_d_1/a_2\_a_1 \times 1000 \quad (1)$$

where $d_{1\text{-}2}$ are consecutive depths at 1-cm intervals and $a_{1\text{-}2}$ are mean model ages. 95% confidence ranges are also calculated using the same equation but $a_{1\text{-}2}$ here represents lower and upper 95% CI. This approach was adopted in our linear, polynomial and P-Sequence models. Despite its wide-range use (Újvári et al. 2017) the adoption of such equations may be suboptimal (Blaauw et al. 2018). Bacon however deals with variability in accumulation rates (sedimentation times in years/cm) through defining prior distributions. As such accumulation rates for any depth of the core are estimated by MCMC iterations providing more realistic views on precision and accuracy too (Blaauw and Heegaard 2012; Blaauw et al. 2018).

Újvári et al. (2017) reports sedimentation times for various Hungarian loess/paleosol profiles dated to MIS 2 and 3, including our study site as well. In their approach, Equation (1) is adopted in such way, that only the overall thickness of the profiles and the two boundary ages is used for the calculations. In our work sedimentation times with 95% CI were calculated using the accrate.depth.ghost function of Bacon for all depths at 1-cm intervals. This function allows to capture varying uncertainties with depth in contrast to Equation (1).

RESULTS

Age-Depth Models

Conventional radiocarbon ages for the studied depth intervals and material type are presented in Table 1. Relying upon the calibrated radiocarbon dates, the base sandy loess is dated to ca. 39 ka cal BP. The overlying loess-paleosol sequence of Madaras was formed between ca. 28 and 12 ka cal BP. Thus, the sequence captures the entire MIS 2 (Andersen et al. 2006; Kreveld et al. 2000; Martinson et al. 1987; Svensson et al. 2006) including the LGM as defined by Clark et al. (2009). Certain authors place the start of the LGM to different times (Denton et al. 1999; Mix et al. 2001; Clark et al. 2009). Based on available paleoecological data (Sümegi 2005; Hupuczi and Sümegi 2010; Bokhorst et al. 2011; Sümegi et al. 2012) it can be placed between 26,000–24,000 cal BP at our site. According to calibrated radiocarbon ages, the base of the profile starts between 39,807 and 38,590 cal BP (95.4%). The development of the first paleosol (MAD-L1S2) overlying the base sands (Figure 1) initiated between 26,570 and 26,009 cal BP years (95.4%) (Table S1). The topmost part of the sequence corresponding to the modern soil must be placed between 13,001 and 12,725 cal BP (Table S1); i.e. preceding the Pleistocene/Holocene transition. The 10-m profile thus spans ca. 16,000 years, rendering an overall average temporal resolution of 16 yr/cm.

Figure 2 presents the results of the linear fit, polynomial, P_Sequence (OxCal), Bacon 1 and 2 models with their 95% confidence ranges. All models display a similar trend. There is no significant difference between the point estimate mean ages of the individual models (see Tables 2, 3, S2). The average, minimum and maximum of mean 2σ error as well as 95% CI ranges of age estimate of the linear model (Table 2) is considerably lower than those of the polynomial and P_Sequence models. The average 2σ error is 192 years in contrast to the 404 years of the polynomial and 533 years of the P_Sequence models. The 95% CI range is 384 years with a minimum of 229 years at the depth of 18 cm and a maximum of 1187 years at the depth of 998 cm for the linear model (Table 2, Figure 2), where dates approach the maximum limit of ^{14}C dating. The average 95% CI range of the polynomial model is much higher (686 years). The minimum value is nearly the same (246 years) to the previous model (Table 2). The maximum value of 1537 years is found at the bottom of the profile at the depth of 980 cm. Furthermore, while the second maximum value of 1490 years is found at the top, the minimum is located ca. 4 m below the top of the profile. Based on this observation regarding precision, the polynomial model can be excluded from our selection of age-depth model choices.

The average, minimum and maximum of 95% CI ranges of age estimate of the P_Sequence (OxCal) model (Table 2) is almost twofold of the values of the previous two models. So, the P_Sequence model is likewise less optimal in terms of chronological precision.

For Bacon models priors on accumulation rates (acc. shape:1.2 acc. mean: 20 year/cm) are very close to the posterior accumulation rates (Figure 2). Moderate (0.5–0.6) memory values indicate a somewhat variable rate of sediment accumulation, which is congruent with our understanding of dust deposition and loess formation (Figure 2). However, for Bacon model 1, both the average, minimum and maximum 2σ errors are higher than the P_Sequence and Bacon 2 models (Table 3). 95% CI is likewise wider for Bacon model 1 than the other two mentioned. In addition, the widest CI and 2σ error values are constrained to the uppermost and lowermost part of the sequence (Figure 2, Table 3). This is not the case for Bacon model 2. In this model the highest mean 2σ error and 95%

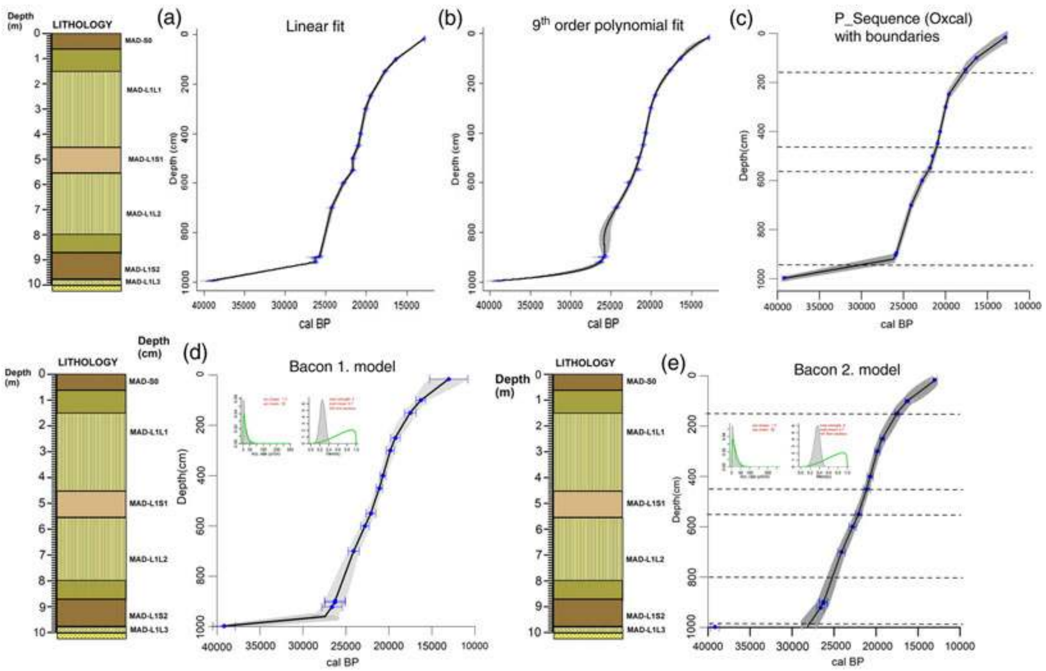

Figure 2 Comparison of constructed age-depth models (squares represent mean values of ^{14}C dated horizons included in the model, solid lines represent mean values, dotted lines and whiskers correspond to 95% confidence intervals).

confidence range values are confined to the bottom of the profile similarly to the P_Sequence model (Figure 2, Tables 2–3). However, the P_Sequence model could not handle ages properly beyond the depth of 9.22 m and yielded a simple linear interpolation with the calibrated date of the paleosol bedrock (MAD-L1L3) at the depth of 9.66 m (Figure 2) similarly to the linear and polynomial age-depth models. Bacon model 2, where a stratigraphic boundary has been introduced just above the bedrock could interpolate data down to this horizon (Figure 2, Table 3) implying that the deposition of the bedrock sands is much older than the overlying loess sequence. Differences in interpolated mean values between Bacon models 1 and 2 is negligible (Table 3) apart from the uppermost modern soil part, where both mean 2 σ error and 95% CI ranges are extremely high in model 1 (Figure 2, Table 2). Differences in mean age values between the two models is the minimal for the lower (MAD-L1L2) and upper (MAD-L1L1) loess packs (Table 3). The highest differences are noted for the lowermost paleosol horizon (MAD-L1S2), the modern soil (MAD-S0) as well as the weakly developed paleosol horizon (MAD-L1S1) intercalated between the older and younger loess packs. Mean 2σ error and 95% CI ranges are almost twofold in Bacon model 1 compared to Bacon model 2. When we compare the output of all models mean 2σ error and 95% CI ranges are the lowest in the linear and Bacon 2 models (Tables 2 and 3). These two models seem to have the highest chronological precision. But as previously stated, linear models tend to underestimate uncertainty (Blaauw et al. 2018). As Bacon models take into consideration the chronological ordering by providing a priori accumulation rates, comparing these with those of the model output can help us assess the "accuracy" of the model. As both the a priori and posterior accumulation rates are very similar in Bacon model 2 (Figures 2 and S1), this model seems to be ideal to realistically mimic sediment

Table 2 Calendar dates received via simple calibration placed into linear, polynomial and P_Sequence (OxCal) models.

	Linear (95.4%)					Polynomial (95.4%)					P_Sequence (OxCal) with boundaries (95.4%)					
Depth (cm)	Mean	Mean 2σ error	95% CI −	95% CI+	95% CI ranges	Mean	Mean 2σ error	95% CI −	95% CI+	95% CI ranges	Mean	Mean 2σ error	95% CI −	95% CI+	95% CI ranges	Stratigraphy
16	12869	136	12733	13004	271	12800	745	12055	13545	1490	12877	295	12582	13172	590	**MAD-SO**
100	16358	190	16168	16547	379	16355	191	16165	16546	381	16311	356	15955	16667	712	
150	17704	222	17482	17926	444	17734	215	17519	17949	430	17612	448	17164	18060	896	
250	19483	191	19292	19674	382	19492	165	19327	19658	331	19577	400	19177	19977	800	**MAD-L1L1**
300	20068	219	19849	20288	439	20044	154	19890	20199	309	19990	303	19687	20293	606	
400	20701	183	20518	20884	366	20702	123	20579	20825	246	20660	266	20394	20926	532	
450	20991	226	20765	21218	453	21003	145	20858	21147	289	20963	347	20616	21310	694	**MAD-L1S1**
500	21622	218	21404	21839	435	21416	172	21244	21588	344	21508	422	21086	21930	844	
550	21682	206	21476	21888	412	21987	198	21789	22185	396	21888	404	21484	22292	808	
600	22798	238	22560	23036	476	22613	237	22376	22849	473	22767	455	22312	23222	910	**MAD-L1L2**
650	23535	173	23362	23707	345	23403	235	23168	23638	470	23421	584	22837	24005	1168	
700	24253	245	24008	24497	489	24331	235	24096	24565	469	24079	410	23669	24489	820	
750	24623	188	24435	24811	376	25170	438	24732	25608	961	24518	510	24008	25028	1020	
800	24994	154	24840	25147	307	25678	675	25003	26352	1349	24984	524	24460	25508	1048	
850	25362	152	25210	25514	304	25744	643	25101	26386	1285	25422	455	24967	25877	910	
870	25510	161	25349	25671	322	25733	491	25242	26224	982	25614	393	25221	26007	786	**MAD-L1S2**
898	26017	297	25720	26314	594	25891	194	25697	26085	388	25834	275	25559	26109	550	
904	26321	448	25873	26770	897	25971	190	25781	26161	380	25959	325	25634	26284	650	
922	26646	269	26377	26915	538	26546	373	26173	26919	746	26163	379	25784	26542	758	
980	36488	468	36020	36955	935	34030	769	33262	34799	1537	26163	379	25784	26542	758	
998	39216	594	38622	39809	1187	39206	577	38629	39782	1153	39167	628	38539	39795	1256	**MAD-L1L3**
Average*		191.95			384		404			686		533			1065	
Min*		114			229		190			246		266			532	
Max*		594			1187		768.5			1537		1356			2712	
SD*		70.46			140.85		261			261		242.99			485.9	
SK		3.142			3.147		1.323			1.323		1.86			1.86	
K		33.25			11.68		1.70			1.70		3.36			3.36	

*Values based on 982 data at 1-cm intervals.

Table 3 Dates received for Bacon models 1. and 2. (without and with stratigraphic boundaries included) and differences in mean, mean 2σ error and 95% CI ranges.

	Bacon model 1. (95.4%)					Bacon model 2. with boundaries (95.4%)					Differences			
Depth (cm)	Mean	Mean 2σ error	95% CI −	95% CI+	95% CI ranges	Mean	Mean 2σ error	95% CI −	95% CI+	95% CI ranges	Mean	Mean 2σ error	95% CI ranges	Stratigraphy
16	13053	2221	10832	15274	4442	12943	263	12680	13206	526	110	1958	3916	**MAD-SO**
100	16289	559	15730	16848	1118	16283	272	16011	16555	544	6	287	574	
150	17505	666	16839	18171	1332	17512	327	17186	17839	653	−7	340	679	
250	19250	547	18703	19797	1094	19245	278	18968	19523	555	5	270	539	**MAD-L1L1**
300	19843	482	19361	20325	964	19847	245	19603	20092	489	−4	238	475	
400	20699	349	20350	21048	698	20706	178	20528	20884	356	−7	171	342	
450	21104	390	20714	21494	780	21116	192	20924	21308	384	−12	198	396	**MAD-L1S1**
500	21625	411	21214	22036	822	21629	204	21426	21833	407	−4	208	415	
550	22091	555	21536	22646	1110	22118	281	21838	22399	561	−27	274	549	
600	22787	494	22293	23281	988	22784	248	22537	23032	495	3	247	493	**MAD-L1L2**
650	23443	652	22791	24095	1304	23447	324	23124	23771	647	−4	328	657	
700	24100	644	23456	24744	1288	24104	328	23776	24432	656	−4	316	632	
750	24655	833	23873	25539	1666	24653	414	24240	25067	827	2	419	839	
800	25202	984	24314	26282	1968	25197	486	24712	25683	971	5	498	997	
850	25746	1113	24792	27018	2226	25723	538	25186	26261	1075	23	575	1151	
870	25965	1138	25033	27309	2276	25940	562	25378	26502	1124	25	576	1152	**MAD-L1S2**
898	26250	1186	25064	27436	2372	26224	582	25643	26806	1163	26	605	1209	
904	26296	1191	25105	27487	2382	26269	583	25686	26852	1166	27	608	1216	
922	26617	1193	25424	27810	2386	26591	571	26020	27162	1142	26	622	1244	
980	27867	1698	26393	29789	3396	27838	814	27024	28652	1628	29	884	1768	
998	39181	1312	37869	40493	2624	39181	656	38706	40018	1312	0	656	1312	**MAD-L1L3**
Average*		817			1634		381			762				
Min*		349			698		176			352				
Max*		2221			4442		863			1725				
SD*		428			855		162			323				
SK		1.36			1.36		0.95			0.95				
K		1.28			1.28		0.15			0.15				

*Values based on 982 data at 1-cm intervals.

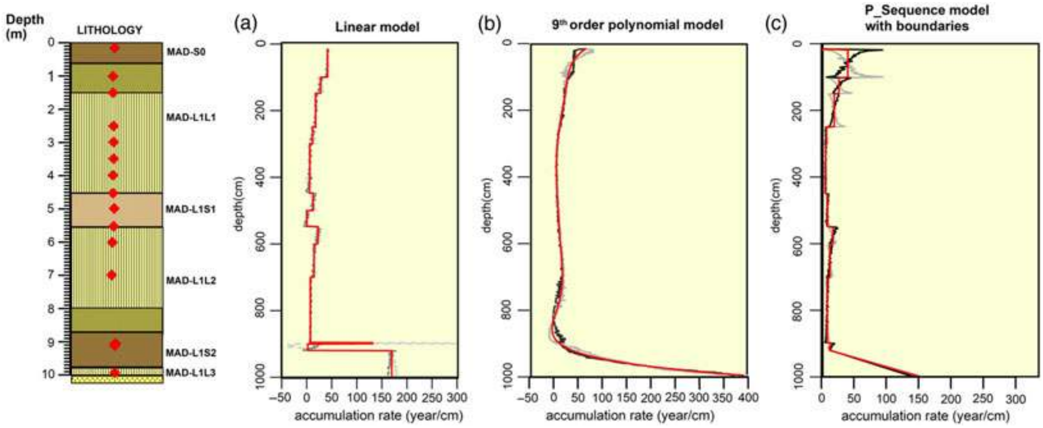

Figure 3 Comparison of calculated sedimentation times (yr/cm) of the linear, polynomial and P-Sequence age-depth models with the observed stratigraphy (red lines: mean values, grey and black lines: 95% confidence ranges). (Please see electronic version for color figures.)

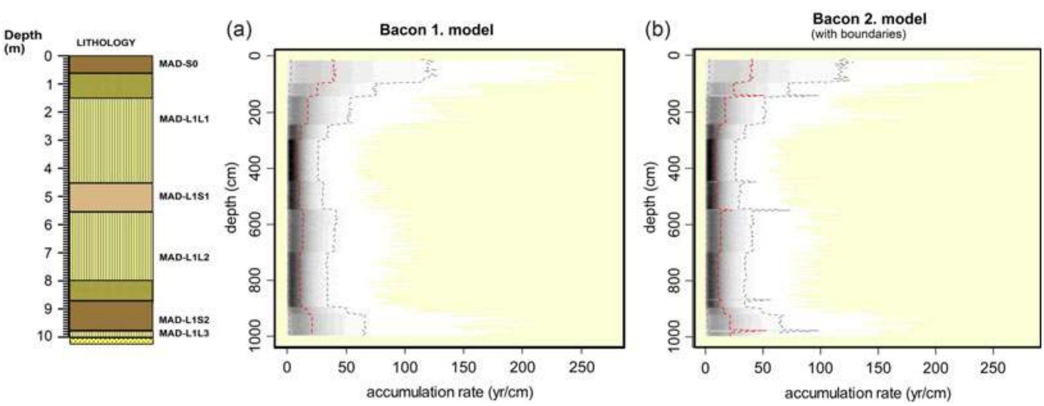

Figure 4 Comparison of calculated sedimentation times (yr/cm) of the Bacon age-depth models with the observed stratigraphy (red dotted lines: mean values, grey dotted lines: 95% confidence ranges, grey shading: probabilities with darker values corresponding to higher probabilities).

accumulation both in terms of precision and accuracy. This model is also the one that best captures the observed stratigraphy; i.e. most accurate.

To further assess the accuracy of the models, sedimentation times per depth profile were created for all age-depth models (Figures 3 and 4). Here all models seem to handle well the observed lithological changes of our profile with the exception of the polynomial model. Stepwise changes are comparable in the rest of the models. Yet both the linear and the P_sequence model does not handle sedimentation times correctly beyond the depth of 9 m (Figure 3), where a progressive aging of the lowermost paleosol unit is postulated towards the base sands. This is in high contrast with our understanding of site evolution seen from the lithostratigraphy. Both Bacon models presume a uniform start of loess deposition much later than the bedrock sand (Figures 2 and 4). This assumption seems more realistic than

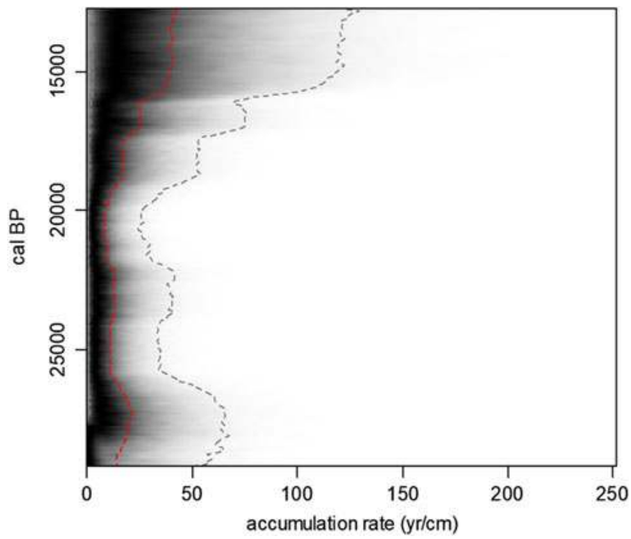

Figure 5 Calculated sedimentation times (yr/cm) against age using the Bacon 2 model (red dotted lines: mean values, grey dotted lines: 95% confidence ranges, grey shading: probabilities with darker values corresponding to higher probabilities).

the others. In addition, the close resemblance of a priori and posterior accumulation times in both Bacon models further corroborates our choice of the most "precise and accurate" model (Bacon 2).

Sedimentation Rates Compared to Other Coeval Sites of the Carpathian Basin

For the entire LPS of Madaras mean sedimentation time was 16.8 yr/cm (15–18 yr/cm 95% CI) based on mid-point estimates calculated for 1-cm intervals using Bacon model 2 (Figure 5). Compared to other records in the literature (Újvári et al. 2017) this is somewhat lower than the one at Dunaszekcső (13.3 yr/cm) spanning a period from ca. 36–23.4 kyr cal BP. It must be noted though that the age-span of the two profiles are only partially overlapping. Furthermore, the average resolution of 13.3 yr/cm published for Dunaszekcső was calculated from the overall thickness of the entire sequence and the bracketing calibrated ^{14}C ages (Újvári et al. 2017). When mean values are recalculated using mid-point estimates for data presented for 1-cm intervals by Újvári et al. (2017), there is an increase to 15.8 yr/cm. Using this data, the difference in sedimentation times between the two sites is negligible (1 yr). So, sampling intervals at 2 and 4 cm will likewise yield similar resolution of 32 and 65 years at Dunaszekcső and 33–68 years at our site of Madaras for the timespan of the entire profile. However, Újvári et. al (2017) used Equation 1 for presenting sedimentation times and accumulation rates in their profile. Despite the adoption of Bacon in the construction of their age-depth model, no evaluation of chronological precision and accuracy of sedimentation times is presented in a way done in our work.

For the period between 28 and 21 kyr, sedimentation times are quite similar along with the overall thickness of corresponding deposits at various sites of the Carpathian Basin (Table S3): Krems (14.5 yr/cm–4.7 m) (Lomax et al. 2014), Süttő (18.3 yr/cm–3.45 m) (Novothny et al. 2011) Tokaj (12.2 yr/cm–4.6 m) (Schatz et al. 2012), Dunaszekcső (11.7 yr/cm–4.36 m) (Újvári et al. 2017), and

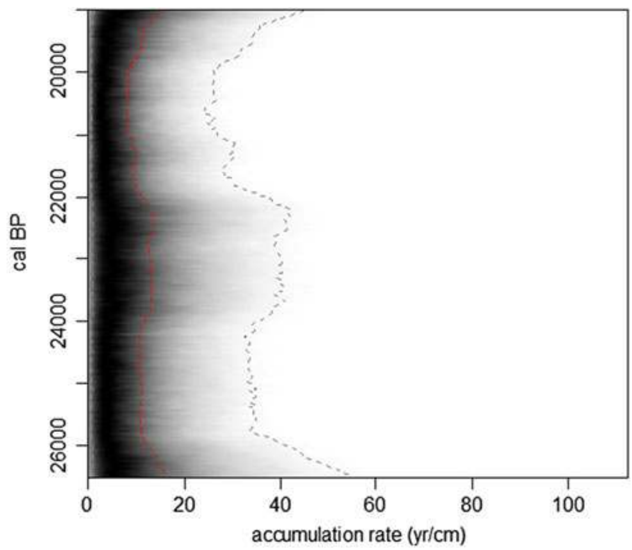

Figure 6 Calculated sedimentation times (yr/cm) against age using the Bacon 2 model for the period of the Last Glacial Maximum (red dotted lines: mean values, grey dotted lines: 95% confidence ranges, grey shading: probabilities with darker values corresponding to higher probabilities).

our study site of Madaras (11.63 yr/cm–4.87 m) (Table S3). This implies relatively uniform conditions responsible for dust accumulation at first sight. However, for accurate evaluation temporal fluctuations should also be considered.

For the LGM part, which represents 70% of the entire LPS at Madaras, mean sedimentation time is even better: 11.63 yr/cm (11–12 cm/yr 95% CI) (Figure 6). Thus, sampling at intervals of 2 cm will yield us a resolution of ca. 23 yr per sample. 4 cm interval samples will still result in a sub-centennial resolution of 48 yr. Considering the total thickness of 6.8 m corresponding to the LGM (Figures 2 and 5), our study site seems to be the best resolved for the LGM in the Middle Danube region.

Average sedimentation rate (ASR) for the entire profile is 0.79 mm/yr (95% CI: 0.8–0.86 mm/yr) with the highest value of 1.43 mm/yr (95% CI: 1.33–1.54 mm/yr) recorded at 21.34 kyr cal BP based on mid-point estimates of the Bacon model 2 (Figures 5 and 6). This value is threefold of that presented by Újvári et al. (2010) (0.25 mm/yr) implying an unusually high dust accumulation at the site (average BMAR: 1183 $g \times cm^{-2} \times kyr^{-1}$ 95% CI: 849–1098 $g \times cm^{-2} \times kyr^{-1}$). The highest recorded value of 2143 $g \times cm^{-2} \times kyr^{-1}$ is confined to the nadir of the LGM. These new values are comparable to but somewhat lower than those recorded for the site of Dunaföldvár between 28.35 and 23.45 kyr b2k (1.002 mm/yr 95% CI: 1.132–1.34 mm/yr, 1504 $g \times cm^{-2} \times kyr^{-1}$ 95% CI: 1699–2024 $g \times cm^{-2} \times kyr^{-1}$) (Újvári et al. 2010 2017). This site is found ca. 40–50 km to the west of our site. However, SR and BMAR values are significantly higher at Madaras for the period of the LGM, which represents 70% of the entire LPS: SR = 0.96 mm/yr 95% CI:0.95–1.01 yr/mm and BMAR = 1404 $g \times cm^{-2} \times kyr^{-1}$ 95% CI:1420–1516 $g \times cm^{-2} \times kyr^{-1}$, respectively.

CONCLUSION

The 10-m loess/paleosol sequence of Madaras brickyard spans ca. 16 kyr of the latest phase of the last glacial. According to previous lithostratigraphic, sedimentological, chronological investigations (Sümegi et al. 2012), the site was characterized by a strong variability of loess deposition and pedogenesis during the past ca. 28 ka cal BP. Dust accumulation and soil formation must have been in a highly fragile equilibrium mostly confined to the border zone during the formation of the entire sequence. Based on our findings Bacon model 2, including information on the visually identified stratigraphic boundaries, performed the best in achieving chronological precision for constructing a reliable chronology of the site. This model allowed for increased uncertainty between dated points, in light with our general understanding on lack of information but managed to constrain uncertainty to an acceptable level. It was also this model that most accurately captured the variability of sedimentation rates with varying uncertainties along the profile. This is a major advent in contrast to the use of generally accepted equations for calculating accumulation rates. The chosen model managed to mimic accumulation rates in terms of the observed stratigraphy and a priori determined sedimentation rates allowing for higher uncertainties at depths close to the bedrock and the modern soil.

The highest accumulation rates are put to the LGM, especially to its nadir. Newly calculated MAR and SR values are much higher than those published by Újvári et al. (2010) for the Carpathian Basin for the period of MIS 2. This must be an artefact of very few dates used by Újvári et al. (2010) on the one hand. Furthermore, in their work linear age-depth models without model and dating uncertainties have been adopted. A recently published work presents accumulation rates for the site of Dunaszekcső (Újvári et al. 2017) gained using Bayesian age-depth models in building a chronology. These are in the same range as those gained by our work. However, in contrast to our study, Újvári et al. (2017) failed to use the sedimentation times yielded by the model itself to assess its "accuracy," as accumulation rates are calculated using simple linear functions.

ACKNOWLEDGMENTS

Research has been carried out within the framework of University of Szeged, Interdisciplinary Excellence Centre, Institute of Geography and Earth Sciences, Long Environmental Changes Research Team. Support of Grants 20391-3/2018/FEKUSTRAT and GINOP-2.3.2-15-2016-00009 'ICER' are acknowledged by the European Union and the State of Hungary, Ministry of Human Capacities, co-financed by the European Regional Development Fund.

SUPPLEMENTARY MATERIAL

To view supplementary material for this article, please visit https://doi.org/10.1017/RDC.2019.154

REFERENCES

An Z, Liu T, Lu Y, Porter SC, Kukla G, Wu X, Hua Y. 1990. The long-term paleomonsoon variation recorded by the loess-paleosol sequence in Central China. Quaternary International 7–8, 91–95.

Andersen KK, Svensson A, Johnsen SJ, Rasmussen SO, Bigler M, Röthlisberger R, Ruth R, Siggaard-Andersen M-L, Steffensen JP, Jensen DD, Vinther BM. 2006. The Greenland ice core chronology 2005, 15–42ka. Part 1: Constructing the time scale. Quaternary Science Reviews 25:3 246–3257.

Bennett KD. 1994. Confidence intervals for age estimates and deposition times in late-Quaternary sediment sequences. Holocene 4:337–348.

Blaauw M. 2010. Methods and code for classical age-modeling of radiocarbon sequences. Quat. Geochronol. 5:512–518.
Blaauw M, Christen JA. 2011. Flexible paleoclimate age-depth models using an autoregressive gamma process. Bayesian Analysis 3:457–474.
Blaauw M, Christen JA, Benett KD, Reimer PJ. 2018. Double the dates and go for Bayes-Impacts of model choice, dating density and quality of chronologies. Quaternary Science Reviews 188:58–66.
Blaauw M, Heegaard E. 2012. Estimation of age-depth relationships. In: Birks HJB, Juggins S, Lotter A, Smol JP, editors. Tracking environmental change using lake sediments, developments in paleoenvironmental research 5. Dordrecht: Springer. p. 379–413.
Bokhorst MP, Vandenberghe J, Sümegi P, Lanczont M, Gerasimenko NP, Matviishina ZN, Markovic SB, Frechen M. 2011. Atmospheric circulation patterns in central and eastern Europe during the Weichselian Pleniglacial inferred from loess grain-size records. Quaternary International 234:64–72.
Bronk Ramsey C. 2009. Bayesian analysis of radiocarbon dates. Radiocarbon 51:337–360.
Clark PU, Dyke AS, Shakun JD, Carlson AE, Clark J, Wohlfahrt B, Mitrovica JX, Hostetler SW, McCabe M. 2009. The Last Glacial Maximum. Science 325:710–714.
Denton GH, Hausser CJ, Lowell TW, Moreno PI, Andersen BG, Heusser LE, Schluchter C, Marchant DR. 1999. Interhemispheric linkage of paleoclimate during the last glaciation. Geographica Annales, Series A, Physical Geography 81A:107–153.
Hertelendi E, Csongor É, Záborszky L, Molnár I, Gál I, Győrffy M, Nagy S. 1989. Counting system for high precision C-14 dating. Radiocarbon 32: 399–408.
Hertelendi E, Sümegi P, Szöőr G. 1992. Geochronologic and paleoclimatic characterization of Quaternary sediments in the Great Hungarian Plain. Radiocarbon 34:833–839.
Hupuczi J, Sümegi P. 2010. The Late Pleistocene paleoenvironment and paleoclimate of the Madaras section (South Hungary), based on preliminary records from mollusks. Central European Journal of Geoscience 2:64–70.
Kemp RA. 2001. Pedogenic modification of loess: significance for palaeoclimatic reconstructions. Earth-Science Rev. 54:145–156.
Kreveld SV, Sarnthein M, Erlenkeuser H, Grootes P, Jung S, Nadeau MJ, Pflaumann U, Voelker A. 2000. Potential links between surging ice sheets, circulation changes, and the Dansgaard-Oeschger cycles in the Irminger Sea, 60–18 kyr. Paleoceanography 15:425–442.
Lisiecki LM, Raymo ME. 2005. A Pliocene-Pleistocene stack of 57 globally distributed benthic δ18O records, Paleoceanography 20, PA1003. Data archived at the World Data Center for Paleoclimatology, Boulder, Colorado, USA.
Lomax J, Fuchs M, Preusser F, Fiebig M. 2014. Luminescence based loess chronostratigraphy of the Upper Palaeolithic site Krems-Wachtberg, Austria. Quaternary International 351:88–97.
Lu H, An Z. 1998. Palaeoclimatic significance of grain size of loess-paleosol sequence of Central China. Science China Series D 41:626–631.
Martinson D, Pisias MG, Hays JD, Imbrie J, Moore TC, Shackleton NJ. 1987. Age dating and the orbital theory of ice ages: development of a high-resolution 0 to 300,000-year chronostratigraphy. Quaternary Research 27:1–30.
Mix AC, Bard E, Schneider R. 2001. Environmental processes of the ice age: land, oceans, glaciers. Quaternary Science Reviews 20:627–657.
Molnár M, Janovics R, Major I, Orsovszki J, Gönczi R, Veres M, Leonard AG, Castle SM, Lange TE, Wacker L, Hajdas I, Jull AJT. 2013. Status report of the new AMS ^{14}C sample preparation lab of the Hertelendi Laboratory of Environmental Studies (Debrecen, Hungary). Radiocarbon 55:665–676.
Novothny Á, Frechen M, Horváth E, Wacha L, Rolf C. 2011. Investigating the penultimate and last glacial cycles of the Sütto loess section (Hungary) using luminescence dating, high-resolution grain size, and magnetic susceptibility data. Quaternary International 234:75–85
Pécsi M. 1990. Loess is not just the accumulation of dust. Quaternary International 7–8:1–21.
Pigati JS, Quade J, Shanahan TM, Haynes Jr CV. 2004. Radiocarbon dating of minute gastropods and new constraints on the timing of spring-discharge deposits in southern Arizona, USA. Palaeogeography. Palaeoclimatology. Palaeoecology 204:33–45.
Pigati JS, Rech JA, Nekola JC. 2010. Radiocarbon dating of small terrestrial gastropod shells in North America. Quaternary Geochronology 5: 519–532.
Pigati JS, McGeehin JP, Muhs DR, Bettis III EA. 2013. Radiocarbon dating late Quaternary loess deposits using small terrestrial gastropod shells. Quaternary Science Reviews 76:114–128.
Porter SC. 2001. Chinese loess record of monsoon climate during the last glacial-interglacial cycle. Earth-Sci. Rev. 54:115–128. doi:10.1016/S0012-8252(01)00043-5.
Porter SC. 2007. Loess records—China. In: Scott AE, editor. Encyclopedia of Quaternary science. Oxford: Elsevier. p. 1429–1440. doi: 10.1016/B0-44-452747-8/00160-5.
Pye K. 1995. The nature, origin and accumulation of loess. Quaternary Science Reviews 14: 653–667.
Reimer PJ, Bard E, Bayliss A, Beck JW, Blackwell PG, Bronk Ramsey C, Buck C, Cheng H, Edwards RL, Friedrich M, Grootes PM, Guilderson TP, Haflidason H, Hajdas I, Hatté C, Heaton TJ, Hoffmann DL, Hogg AG, Hughen KA, Kaiser KF, Kromer B, Manning SW, Niu M, Reimer RW, Richards DA,

Scott EM, Southon JR, Staff RA, Turney CSM, van der Plicht J. 2013. IntCal13 and Marine13 radiocarbon age calibration curves 0–50,000 years cal BP. Radiocarbon 55(4):1869–1887. doi:10.2458/azu_js_rc.55.16947.

Rasmussen SO, Andersen KK, Svensson AM, Steffensen JP, Vinther BM, Clausen HB, Siggaard-Andersen SJ, Larsen LB, Dahl-Jensen D, Bigler M, Rhöthlisberger R, Fischer H, Hansson ME, Ruth U. 2006. A new Greenland ice core chronology for the last glacial termination. Journal of Geophysical Research: Atmospheres 111:D06102. doi:10.1029/2005JD006079

Schatz AK, Buylaert JP, Murray A, Stevens T, Scholten T 2012. Establishing a luminescence chronology for a palaeosol-loess profile at Tokaj (Hungary): A comparison of quartz OSL and polymineral IRSL signals. Quaternary Geochronology 10:68–74.

Sokal RR, Rohlf FJ. 1995. Biometry: the principles and practice of statistics in biological research. New York: W.H. Freeman. 495 p.

Sümegi P. 2005. Loess and Upper Paleolithic environment in Hungary. Aurea Kiadó, Nagykovácsi.

Sümegi P, Hertelendi E. 1998. Reconstruction of microenvironmental changes in Kopasz Hill loess area at Tokaj (Hungary) between 15,000–70,000 BP years. Radiocarbon 40:855–863.

Sümegi P, Gulyás S, Csökmei B, Molnár D, Hambach U, Stevens T, Markovic S, Almond P. 2012. Climatic fluctuations inferred for the Middle and Late Pleniglacial (MIS 2) based on high-resolution (ca 20yr) preliminary environmental magnetic investigation of the loess section of the Madaras brickyard. Central European Geology 55:329–345.

Svensson A, Andersen KK, Bigler M, Clausen HB, Dahl-Jensen D, Davies SM, Sigfus JJ, Muscheler R, Rasussen SO, Rhöthlisberger R, Steffensen JP, Vinther BM. 2006. The Greenland ice core chronology 2005, 15–42ka. Part 2: comparison to other records. Quaternary Science Reviews 25:3258–3267.

Telford RJ, Heegaard E, Birks HJB. 2004. All age-depth models are wrong: but how badly? Quaternary Science Reviews 23:1–5.

Trachsel M, Telford RJ. 2017. All age-depth models are wrong, but are getting better. Holocene 27: 860–869.

Újvári G, Kovács J, Varga G, Raucsik B, Marković SB. 2010. Dust flux estimates for the Last Glacial Period in East Central Europe based on terrestrial records of loess deposits: a review. Quaternary Science Reviews 29:3157–3166.

Újvári G, Molnár M, Novothny Á, Páll-Gergely B, Kovács J, Várhegyi A. 2014. AMS ^{14}C and OSL/IRSL dating of the Dunaszekcső loess sequence (Hungary): chronology for 20 to 150 ka and implications for establishing reliable age-depth models for the last 40 ka. Quaternary Science Reviews 106:140–154.

Újvári G, Stevens T, Molnár M, Demény A, Lambert F, Varga G; Timothy AJ, Páll-Gergely B, Buylaert JP, Kovács J. 2017. Coupled European and Greenland last glacial dust activity driven by North Atlantic climate. PNAS 114(50): 10632–10638.

Xu B, Gu Z, Han J, Hao Q, Lu Y, Wang L, Wu N, Peng Y. 2011. Radiocarbon age anomalies of land snail shells in the Chinese Loess Plateau. Quaternary Geochronology 6:383–389.

Vandenberghe J. 1985. Paleoenvironment and stratigraphy during the last glacial in the Belgian-Dutch border region. Quaternary Research 24: 23–38.

Woillard G, Mook W. 1982. Carbon-14 dates at Grande Pile: correlation of land and sea-chronologies. Science 215:159–161.